energies

Review

Review of the Liquid Hydrogen Storage Tank and Insulation System for the High-Power Locomotive

Daehoon Kang [1,*], Sungho Yun [2] and Bo-kyong Kim [1]

[1] Smart Electrical & Signaling Division, Korea Railroad Research Institute, Uiwang 16105, Korea; bkkim@krri.re.kr
[2] Railroad Safety Division, Korea Railroad Research Institute, Uiwang 16105, Korea; hadogo@krri.re.kr
* Correspondence: kkangdh89@gmail.com

Abstract: Hydrogen has been attracting attention as a fuel in the transportation sector to achieve carbon neutrality. Hydrogen storage in liquid form is preferred in locomotives, ships, drones, and aircraft, because these require high power but have limited space. However, liquid hydrogen must be in a cryogenic state, wherein thermal insulation is a core problem. Inner materials, including glass bubbles, multi-layer insulation (MLI), high vacuum, and vapor-cooled shields, are used for thermal insulation. An analytic study is preferred and proceeds liquid hydrogen tanks due to safety regulations in each country. This study reviewed the relevant literature for thermodynamic modeling. The literature was divided into static, dynamic, and systematic studies. In summary, the authors summarized the following future research needs: The optimal design of the structure, including suspension, baffle, and insulation system, can be studied to minimize the boil-off gas (BOG). A dynamic study of the pressure, mass flow, and vaporizer can be completed. The change of the components arrangement from the conventional diesel–electric locomotive is necessary.

Keywords: liquid hydrogen; hydrogen tank; insulation; cryogenics

check for updates

Citation: Kang, D.; Yun, S.; Kim, B.-k. Review of the Liquid Hydrogen Storage Tank and Insulation System for the High-Power Locomotive. *Energies* **2022**, *15*, 4357. https://doi.org/10.3390/en15124357

Academic Editors: Hyun-Goo Kim and Youngkuk Kim

Received: 9 May 2022
Accepted: 13 June 2022
Published: 15 June 2022

1. Introduction

Mobile vehicles require independent energy carriers, for which alternatives to fossil fuels, such as batteries and hydrogen, are currently under research and development, as shown in Table 1. Electric propulsion systems using motors have been gradually introduced into the large transportation sector, such as trains, ships, and aircraft. Therefore, the vehicles can be arranged according to the required power. Conventional internal combustion engines (ICEs) or fuel cells can be viewed as power generators.

Hydrogen can be stored in gaseous, liquid, or chemical forms [1]. Metal hydrate, which can store and take out hydrogen through a thermal reaction, has also been researched [2]. Liquid organic hydrogen carriers (LOHCs) and ammonia, which are chemical forms, have the advantages of safe use but are not suitable for vehicles, because they require large-volume equipment to input energy for conversion. Gaseous hydrogen storage provides a fast response, but the energy content per weight and volume remains low, even if the tank pressure is high (350–700 bar). The liquid hydrogen (LH_2) form has the highest energy density and can be easily converted to hydrogen gas through a vaporizer. Hence, LH_2, rather than gaseous hydrogen, could be preferred as a fuel for vehicles requiring a high-speed rail or enormous power. The use of LH_2 saves space and reduces the locomotive's weight, allowing more cargo to be loaded.

The battery's energy density is 300–500 Wh/kg and 700–1000 Wh/L, and the energy density of LH_2 is 2000–2500 Wh/kg and 110–140 Wh/L. Therefore, for the same energy storage system (ESS), hydrogen is lighter in weight than the battery, and the battery is smaller in volume than hydrogen. Due to these characteristics, batteries are considered for low-powered vehicles with a relatively short mileage, whereas hydrogen is considered for high-powered vehicles with a long mileage.

Table 1. Applications and required power and energy storage amounts.

Required Power	Application					Form of ESS	
	Stationary	Transportation					
		Vehicle	Ship	Aircraft	Space	Battery	H_2
1–3 kW	House	Bike	Yacht	Drone	Shuttle	~100 kg	-
10–100 kW	Building	Car	Fishboat	Cargo drone	Station	~500 kg	~10 kg (~100 km/kg)
200–400 kW		Self-driving Bus, Truck Railcar	River taxi Submarine	Air mobility Light-craft	Base (Moon, Mars)	~1 ton	~250 kg (~5 km/kg)
1–5 MW	Complex	Locomotive	Ferry Cruise	Helicopter		~10 ton	~1 ton (~1 km/kg)
5–20 MW	Small city		Cargo	Airplane		-	~10 ton

For example, hydrogen or battery trains can replace diesel trains in the train sector. Using catenary lines is energetic and economically efficient, but the electrification rate of the railway is not high worldwide. The electrification rate of Northeast Asia and Europe is over 60%, but the rest of the Earth, including the Americas, Africa, and Australia, is under 10%. As an alternative to the diesel trains operating on routes without catenary lines, battery trains can be used as short-distance trams in cities, and hydrogen trains can be used as multiple-unit or long-distance, high-powered locomotives.

The replacement of diesel trains can be helpful for international environmental regulations. In Korea, 265 diesel locomotives existed as of 2018. They emit air pollutants equivalent to 300 commercial diesel vehicles. By converting diesel locomotives to hydrogen locomotives, direct air pollutants (particulate matter (PM)) and indirect air pollutants (CO and NO_x) are expected to be reduced.

Hydrogen trains have been actively studied since the commercialization by Alstom in France in 2014, and their model 'Coradia iLint' was unveiled in 2016. Beyond the railcar and tram, hydrogen locomotive and shunter have been researched by CP in Canada, CRRC in China, CZ in the Czech Republic, PESA in Poland, Wabtec in the United States, and Korean Railroad Research Institute (KRRI), as shown in Table 2. Especially, KRRI is working on the world's first LH_2 locomotive.

Table 2. Recent cases of hydrogen trains.

Type	Year	Institution	Power (Fuel Cell)	Hydrogen	Mileage	Note
Railcar	2016	Alstom (France)	390 kW (250 kW)	250 kg	1000 km	Commercial
	2017	CRRC (China)	200 kW (200 kW)	12 kg	40 km	Commercial
	2021	KRRI (Korea)	200 kW (200 kW)	166 kg	600 km	
	2022	Siemens (Germany)	400 kW (400 kW)	-	800 km	
	2022 (target)	JR East (Japan)	240 kW (240 kW)	25 kg	140 km	
	2023 (target)	Hyundai (Korea)	400 kW (400 kW)	40 kg	150 km	Tram
Locomotive	2021	PESA (Poland)	600 kW (180 kW)	175 kg	-	Shunter
	2021	CRRC (China)	700 kW (400 kW)	-	627 km	
	2022 (target)	CP (Canada)	1200 kW (1200 kW)	-	-	
	2023 (target)	CZ LOKO (Czech)	800 kW (800 kW)	-	-	Shunter
	2024 (target)	KRRI (Korea)	1800 kW (1200 kW)	70 kg	-	Liquid hydrogen
	-	Wabtec (USA)	-	-	-	

The study of LH_2 storage came under the spotlight in earnest during the space race in 1957. The National Aeronautics and Space Administration (NASA) built the Saturn rocket series using LH_2 as fuel at the Kennedy Space Center (KSC) in Florida, and preliminary tests were conducted at the Marshall Space Flight Center (MSFC) in Alabama. The LH_2

tank requires a high level of thermal insulation to avoid thermal loss. The significant temperature difference between LH_2 (as low as 20 K) and the surrounding atmosphere induces boil-off gas (BOG), which leads to high pressure and the loss of stored hydrogen. In addition to heat leakage, flashing, sloshing (especially after thermal stratification), and ortho-to-parahydrogen conversion can cause boil-off [3]. This study focuses on heat leakage in the static state.

Following the space race, MSFC researched long-term LH_2 storage in the 1990s, rather than temporary storage for a rocket launch, with the NASA Glenn Research Center (GRC) and Lockheed Martin Space Systems [4,5]. The multi-purpose hydrogen test bed (MHTB) included an 18.09 m^3 tank, insulated with a 3.53-cm-thick spray-on foam insulation (SOFI) and a 3.75-cm-thick multi-layer insulation (MLI) with 45 aluminum blankets and spacers, as shown in Figure 1. The MLI was simulated using layer-by-layer, Lockheed, and modified Lockheed models, and the differences in the methods are described in the following Section 2.3 [6]. A vacuum gap separated the outer and inner vessels, and the two vessels were fixed through the ground-hold or orbit-hold method. The results showed a heat leakage of 0.22 W/m^2 for the orbit-hold method and 305 K room temperature, which is 50% less than when no MLI is used. The ground-hold method showed a heat leakage of 63 W/m^2, which is 238 times that of the orbit-hold method. This result shows that the heat conduction at the suspension between the two vessels, which is the structure that maintains the distance between the two vessels and fixes them, is more excellent than the heat leakage of the wall surrounded by insulation schemes. Therefore, this result showed the necessity to study the method of fixing two vessels with minimal structure to avoid heat conduction. Another example of long-term LH_2 storage other than NASA is the first LH_2 fueling station built at Munich Airport in Germany in 1999. However, the LH_2 tank was not directly used to fuel LH_2, and a vaporizer was used to fuel the gas tank vehicles [7].

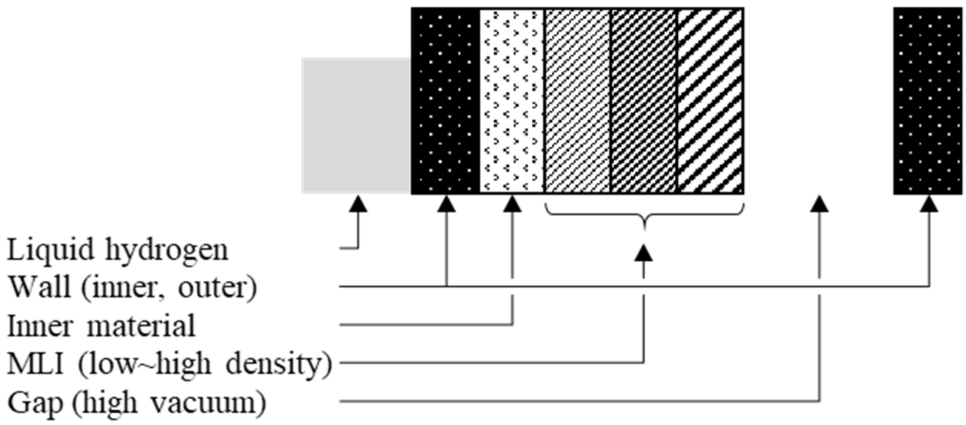

Figure 1. Insulation concept of the multi-purpose hydrogen test bed [4,5].

Following the stationary LH_2 storage, mobile LH_2 vessels have been researched. In 1999, BMW showed the first LH_2 vehicle, 750hl, in Germany. In 2018, Hylium built the first mobile refueling truck in Korea. In 2021, Linde provided LH_2 tanks to Hjelmeland Ferry in Norway.

This study reviewed the literature necessary for the system modeling of LH_2 storage tanks for application in the transportation sector. First, static modeling studies, including heat transfer coefficients and thermal conductivity, were reviewed. Second, dynamic modeling studies were reviewed, including phase changes and values with changes over time. Third, systematic modeling studies for suitable sizing and arrangement of the power system for a vehicle were reviewed. Lastly, the future research needs were summarized.

2. Static Modeling

2.1. Wall, Vacuum Gap, Suspension, and Sensors

Various tank shapes have been studied for ships carrying LNG, and the expression "1st/2nd barrier of the tank" is used instead of "inner/outer vessel" of the LH_2 tank. The tanks are independent or integrated with the ship, which GTT operates in France.

Most materials become brittle under cryogenic conditions, such as stainless steel, aluminum alloy, titanium alloy, and composite materials, whose behaviors have been studied. Grade 316L stainless steel, which has a low carbon content, is commonly used [8]. Stainless steel has a thermal conductivity of approximately 10 W/(m·K) at 20 K in contact with LH_2 and approximately 16 W/(m·K) in contact with the air at room temperature. The thermal resistance equation can represent the inner wall for conduction in a cylindrical form [9].

Other materials, such as copper, which has a poorer insulation effect than steel, can be considered for the inner vessel. The existing studies have only focused on the insulation effect. Instead, the total efficiency should be considered when designing an LH_2 tank for a vehicle. The loss rate through vaporization during storage is approximately 0.1–5% per day, but the loss rate during charging is approximately 20% per charge if the vessel is at room temperature. Moreover, the storage period for a vehicle can be as short as a few days. Therefore, an economic–energetic approach must be formulated to determine the optimal point. The case of charging the vessel containing LH_2 at cold temperatures instead of the empty vessel at room temperature can also be considered.

The air layer in the gap between the inner and outer vessel walls can be configured as the heat conduction of gases and heat radiation between solids. The outer vessel wall was cooled via air convection, and radiation to the surroundings was assumed to be in the same condition as the air. The emissivity of stainless steel is 0.6 (dimensionless), the convective heat transfer coefficient of the air is approximately 2 W/(m^2·K), and the Stefan–Boltzmann number is 5.667×10^{-8} W/(m^2·K^4). The air and surrounding temperatures are generally assumed to be equal.

The suspension structure connects the inner and outer walls, and heat conduction appears. G10, G10-CR, and G11, which are fiberglass, can be used for suspension and supports for small-sized stationary tanks [10]. Their thermal conductivity is approximately 0.2~0.3 W/(m·K). However, 316L stainless steel can be used for a big size of tank for mobility, and it will enlarge the heat leakage.

Sensors also connect the inner and outer walls. Level, pressure, and temperature sensors are typical. Their outer material can be 316L stainless steel, but the wire material can be copper. For insulating the wire, the polyimide film can be used as the shell material, and its thermal conductivity is approximately 0.1~0.7 W/(m·K) by product and temperature.

2.2. Inner Materials

As the inner materials (IMs), porous foam, SOFI, fiber-reinforced plastic (FRP), aerogel, glass bubble, and hollow glass microsphere (HGM) have been used. Polyurethane foam has been used to insulate liquified natural gas (LNG), but a higher insulation performance is required for the insulation of LH_2. A thickness of several meters is required to insulate LH_2 by using polyurethane foam.

Unlike the thermal conductivity of MLI, which changes significantly with the change in the degree of vacuum, the vacuum pressure had little effect on that of SOFI. Fesmire researched the effects of spray foam and rigid foam in non-vacuum conditions for the insulation of the rocket fuel tanks [11]. Johnson et al. tested the heat flux according to the vacuum pressure in MLI for the long-term storage of liquid methane on the lunar surface and suggested a correlation formula [12].

SOFI has a thermal conductivity of 10^{-3}–10^{-2} W/m·K and can be simplified to a hypothetical layer in which the thermal conductivity ranges from 0.005 to 0.04 W/(m·K). Tseng et al. measured the thermal conductivity of polyurethane foam and suggested the shape of the test chamber and the experimental method [13]. Mekonnen et al. described the process from fabrication to coating aerogels and showed the thermal conductivity range [14].

MLI shows a 35–50% better insulation performance than SOFI [15]. By contrast, HGM has a thermal conductivity of 10^{-3}–10^{-4} W/m·K, which is even better than MLI [16,17]. A group of microspheres is easily assumed to be the same size and uniform arrangement, as shown in Figure 2. However, the particle size is all different in an actual experiment, and the accumulation is random.

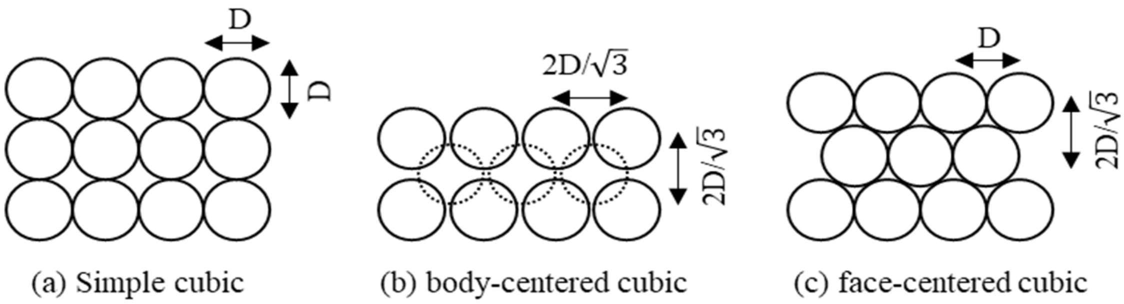

Figure 2. Cubic arrangement of a hollow glass microsphere for insulation [16].

2.3. Multi-Layer Insulation

MLI and variable density MLI (VDMLI) were studied. MLI consists of a reflector with low thermal emissivity and a spacer with low thermal conductivity. Spacers prevent reflectors from direct contact and avoid heat conduction. Alumina-coated polyester sheets, alternating layers of aluminum foil and glass fiber, aluminum, silica, or perlite particles, were used for MLI [18]. Typically, Mylar or Kapton can be used as a reflector, and Dacron nets can be used as the spacer [19]. The external film can be coated by painting or material such as glass-reinforced cloth. An example of MLI for insulating spacecraft is the same in Figure 3 [20].

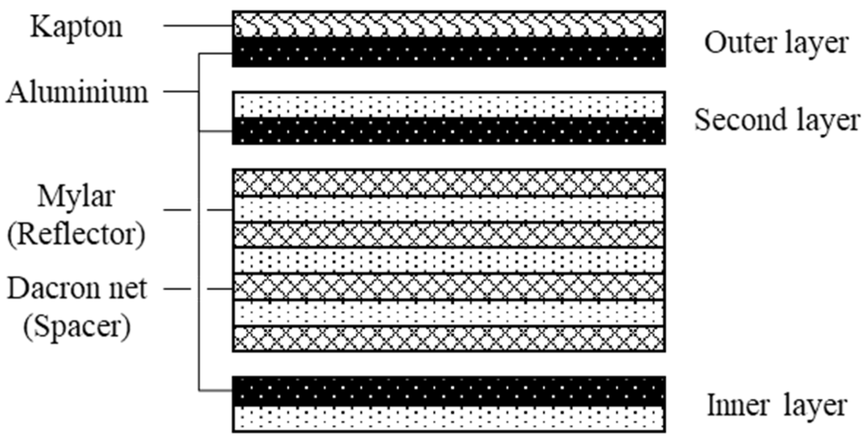

Figure 3. MLI configuration for insulating spacecraft [20].

Previous studies have shown that the ratio of these heat flux components depends on the temperature distribution [21]. Thus, VD-MLI, which allows for the thickness of spacers to be modified, provided a better insulation performance than the basic MLI [22]. Many studies have suggested the optimization of the layer density and arrangement via thermodynamic modeling [23–25]. Optimization based on a combination of foam and MLI was also researched, and the combination of foam and MLI showed a 10–50% higher performance than MLI alone [26,27].

MLI can be simplified to a hypothetical layer in which the thermal conductivity varies from 0.00001 to 0.072 W/(m·K), owing to material differences and pressure variations [28]. MLI can be simulated by layer-by-layer, Lockheed, and modified Lockheed models. The Lockheed model is based on a semi-empirical formula and can quickly solve the overall heat flux, but the selection of empirical parameters depends on the conditions. By contrast, the layer-by-layer method is based on an iterative algorithm and can calculate the temperature of each layer in MLI. The layer-by-layer method divides the heat transfer into three forms: solid heat conduction, gaseous heat conduction, and radiation.

2.4. Phase Change of Liquid Hydrogen

The heat transfer coefficient (HTC), critical heat flux (CHF), and thermal conductivity of the hydrogen have been studied. Kumar et al. solved a homogeneous two-phase model and showed that the effect of evaporation on stratification increases as the aspect ratio, which means the ratio of width and height of the tanks, increases by Ansys Fluent [29]. Horie et al. experimentally summarized the film boiling heat transfer coefficient of LH_2, according to the pressure and the subcooling temperature [30]. Baldwin et al. reviewed the relations related to the pool nucleate boiling and pool film boiling of LH_2, liquid oxygen, and methane [31]. Ganesan et al. derived a universal CHF correlation from a cryogenic flow database from 1959 at Purdue University Laboratory [32]. Kuang et al. summarized the nucleate flow boiling HTC of the LH_2 and suggested the artificial neural network that can derive HTC [33]. Wang et al. performed a numerical study of pool film boiling specific to the horizontal cylinder [34].

Kang et al. suggested a 0-D quasi-steady thermal network model, as shown in Figure 4 [35]. In Figure 4, unlike other studies that modeled only the insulation system, the liquid and gaseous hydrogen were assumed to be a single node with mass, temperature, pressure, and volume. The thermal resistance diagram, including hydrogen, can be expanded to dynamic modeling with venting, filling, and vaporizing, with level and pressure changes in the tank. On the other hand, the study of high-pressure vessels with phase changes is similar to the steam generation heat pump [36]. In the industrial sector, high-temperature and high-pressure steam are used, and heat pumps with higher energy efficiency than boilers are introduced. In a flash tank, water and steam coexist, and water is added as much as steam is used.

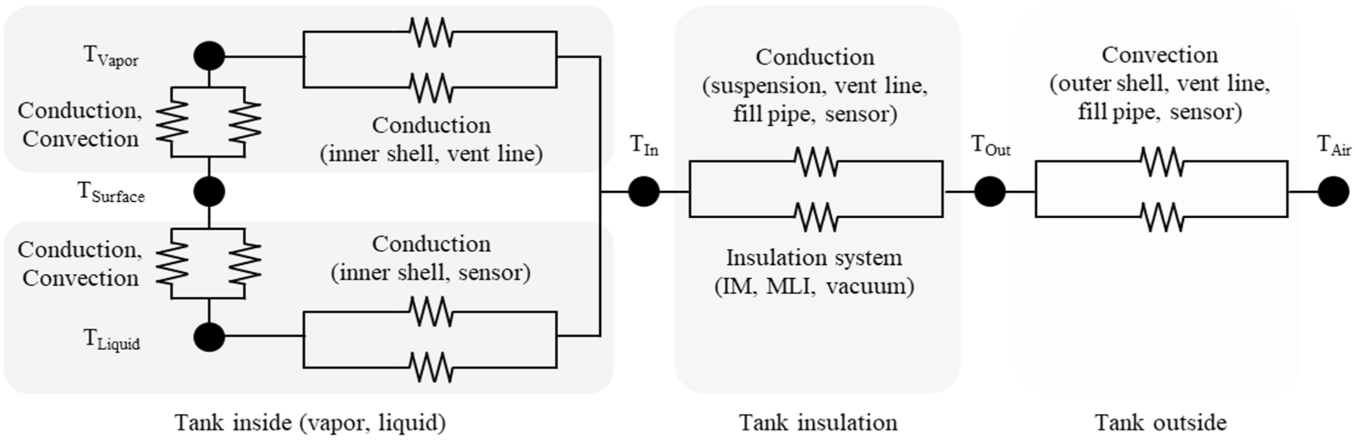

Figure 4. Thermal resistance diagram of a LH_2 insulation tank [35].

3. Dynamic Modeling

3.1. Changes due to Phase Change of the Hydrogen

One of the characteristics of LH_2 is that its sensible heat is more significant than its vaporization heat until it reaches a gaseous state at room temperature. The ratio of the two increases with the increase in pressure, and thus, the effect of the tank pressure was studied. The ratio is 7.82 at 100 kPa and 23.70 at 1.2 MPa [37]. The enthalpy changes by 3860 kJ/kg while vaporizing from –253 to 20 °C, as shown in Table 3 [38]. The heat of the phase change and sensible heat of hydrogen can be obtained using REFPROP (version 10, National Institute of Standards and Technology).

Table 3. Properties of hydrogen.

Temperature (°C)	–253	–253	0	20 [A]	70 [B]
State	Liquid	Vapor	Vapor	Vapor	Vapor
Enthalpy (kJ/kg)	0	480	3580	3860	4580

[A] Room temperature. [B] Operating temperature of fuel cell.

A commercial electrolyzer requires 45–50 kWh of electricity to produce 1 kg of hydrogen, higher than the higher heating value (HHV) of hydrogen (39.4 kWh/kg), and emits 5–10 kWh/kg of heat. A commercial fuel cell generates 15–20 kWh/kg of electricity from 1 kg of hydrogen, which is lower than the hydrogen's lower heating value (LHV) (33.4 kWh/kg) and emits 13–18 kWh/kg of heat. The vaporization heat of LH_2 is insufficient to cool the fuel cell, but it can help insulate the LH_2 tank.

Additionally, the expansion ratio of the vaporization is approximately 848, which means that 100 kPa of LH_2 can be vaporized to 172 MPa of vapor hydrogen. The typical fuel cells for vehicles use 300 kPa–1.6 MPa of gaseous hydrogen. Therefore, appropriate pressure control is required from the vessel to the vaporizer and the fuel cell inlet.

3.2. Vapor-Cooled Shield or Vent Line

A vapor-cooled shield (VCS) is a vent pipe made from the same material as the inner vessel and located between the inner wall and the end of MLI. For production convenience, the VCS can be placed just outside the inner wall by winding around it. The VCS can be simplified to a single layer and considered as intercepting the heat penetration at the middle.

The VCS, which involves recovering the sensible heat of the self-evaporated gaseous hydrogen owing to heat penetration, is a technology at the boundary between passive insulation and active insulation. The insulation effect of the VCS with LH_2, nitrogen, oxygen, and methane was studied using a model validated against the existing experimental data [39]. Subsequently, the optimal location of the VCS within the foam and MLI and its thermal behavior was studied [37,40,41]. In addition, another material, liquid nitrogen, which has a higher boiling point than LH_2, was studied for use as an insulation shield around the LH_2 tank [37].

Based on the energy conservation, the heat transfer in the VCS is the same as the difference in heat entering into and exiting out of the VCS, as illustrated in Figure 5. The heat penetration into the inner tank (Q_{in}) is assumed to be the latent heat of the vaporization of hydrogen. In contrast, the heat transfer through the VCS (Q_{vcs}) is assumed to be sensible heat caused by the difference between the saturated vapor temperature and the outside temperature.

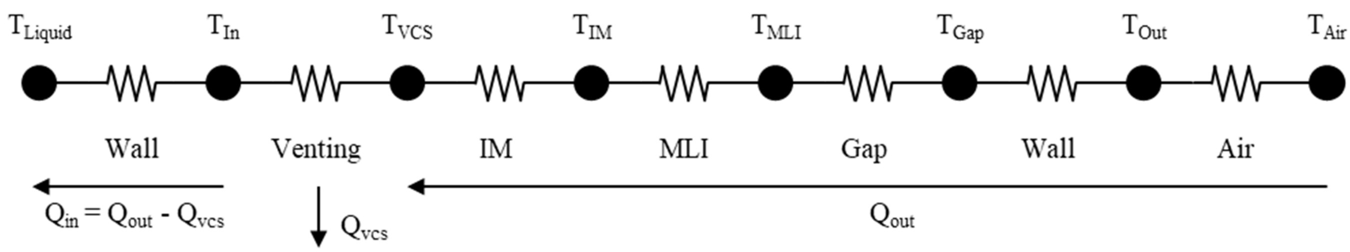

Figure 5. The example of thermal equilibrium and temperature nodes [31–33].

3.3. Boil-Off Ratio

The Boil-off Ratio (BOR) means the ratio of BOG generated in a day from the size of the entire tank. The analysis conditions for the calculation of the BOR are shown in Figure 6. For example, Jeon et al. predicted the BOR of the stationary tanks by a multiphase thermal simulation [42]. A C-type liquid nitrogen tank and membrane LNG tank were analyzed by the computational fluid dynamics (CFD) software STAR-CCM+, and the results showed that heat conduction through suspension is significant.

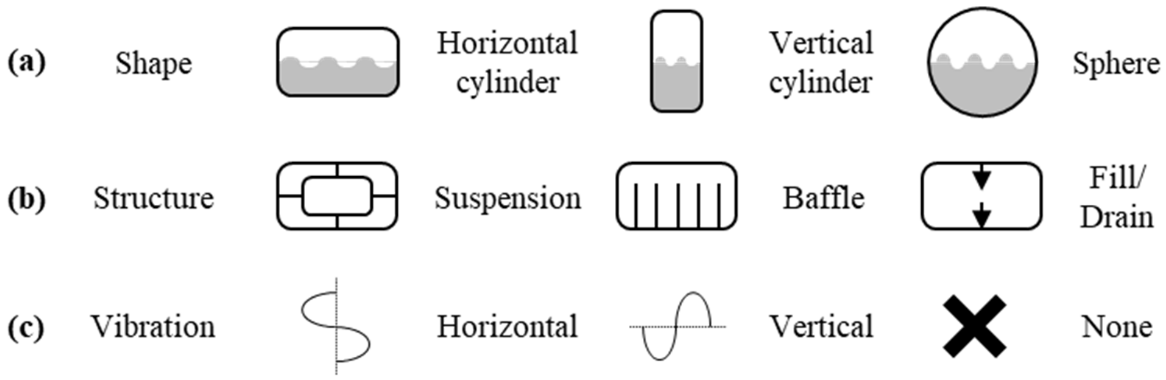

Figure 6. Analysis conditions: (**a**) shape, (**b**) structure, and (**c**) vibration (sloshing).

However, the mobile vessels for transport show a higher BOR due to sloshing by vibration compared to the stationary vessels. Liu et al. did a series of studies on numerical models of dynamic meshes in sloshing conditions [43–45]. The authors used the software ICEM surf with the volume of fluid (VOF) method and applied the horizontal sinusoidal vibration to the LH_2 tank. Slosh baffles in the tank decreased the sloshing, and BOR increased the stratification thickness. The authors additionally studied the force, momentum, pressure, and amplitude of the vibration in sloshing. Wei et al. analyzed the effect of horizontal sinusoidal sloshing on vertical tanks using the software Fluent 17.0 (ANSYS Inc., Pittsburgh, PA, USA) [46]. The authors showed that the pressure–time curve increases if the vibration condition exceeds the critical amplitude and frequency.

Ghafri et al. summarized LH_2 boil-off modeling and implemented it in the software package BoilFAST [47]. The software is validated by multiple sets of industrially relevant data, including NASA, and provides static and dynamic modeling. Besides, the pathway's heat penetration, including pipes and cryopump, was studied. Petitpas et al. showed that the losses along the pathway of LH_2 could vary by up to 15% and calculated an economic-energetic analysis [48].

4. Systematic Modeling

4.1. Capacity of the Power Required and the Fuel Tank

The capacity of the fuel cell and fuel tank are determined according to the purpose of the hydrogen vehicle. The typical capacity ranges of the hydrogen vehicle are listed in Table 4. The Hyundai group in Korea modularized its fuel cells to 100 kW and produced more than 20,000 fuel cells per year. Buses, trucks, and trams require two to four fuel cell modules, whereas locomotives require one to two modules for each of the six wheels. With the increase in the weight, including cargo and passengers, the fuel efficiency decreases, and the size of the fuel tank is determined to meet the required distance according to the purpose of the vehicle.

Table 4. Typical capacity ranges of the fuel cells and fuel tanks of hydrogen vehicles.

	Car (Personal) [A]	**Car (Bus, Truck)** [B]	**Train (Tram)** [C]	**Train (Locomotive)** [D]
Fuel cell (kW)	100	100–200	200–400	2000–4000
Fuel tank (kg)	6–8	30–40	50–250	500–1000
Efficiency (km/kg)	90–100	5–20	1–3	1–2
Distance (km)	600–800	200–1000	200–1000	500–1000

[A] Hyundai Nexo (2018). [B] Hyundai Elec-city Bus (2018) and Xcient Truck (2020). [C] Alstom (2016), CRRC (2017), and Hyundai-Rotem (2021). [D] KRRI (predicted value).

Apart from the vehicles, the LH_2 tank for drones weighs 0.3–1 kg, the ground tank for refueling stations is 20–450 kg, and the trailer tank for transport weighs 1000–3000 kg. The

Saturn V rocket used in the space race carried 69 metric tons of LH_2, but this is not relevant to this study, because its tank was meant for immediate launch and not for insulated storage.

4.2. Arrangement of the Fuel Tank

Smith et al. designed a conceptual LH_2 carrier ship from a conventional LNG carrier ship [49]. Ship sizing, power consumption, including electrified propulsion system and reliquifying the hydrogen system, and sloshing are reviewed. The authors predicted that only 40.2% of energy could be loaded at the same volume, and the fuel loss rate could be reduced by 38.7% through reliquefication.

Similarly, KRRI is considering the arrangement of the LH_2 locomotive from a conventional diesel locomotive. GE PowerHaul is a major diesel–electric locomotive with 2.8 MW power since 2007, and it is called Class 70 in the UK, DE 36000 in Turkey, and Class 7600 in Korea. Its standard subclasses include PH37ACi in mainland Europe and PH37ACmi in the UK. A sample of its configuration is shown in Figure 7. The components related to the engine and mass flow will be changed to the fuel cell and the hydrogen supply system. The heating, ventilation, and air-conditioning (HVAC) system will remain. However, its sizing and arrangement will be changed, because the amount of heat generation for power generation (engine to fuel cell) is different. New technologies, including liquid- or phase-change cooling, can be applied to decrease the volume of the HVAC system.

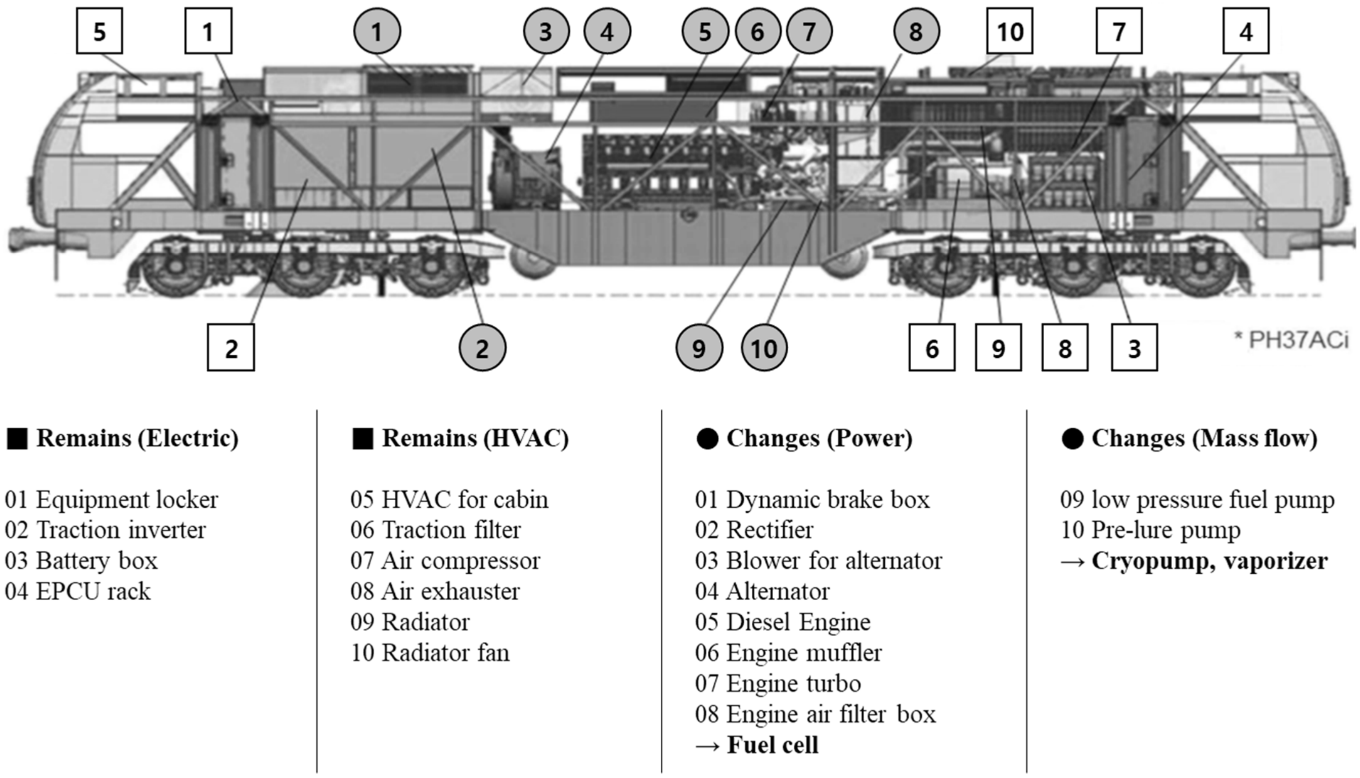

Figure 7. Sample of the configuration of the PH37ACi diesel–electric locomotive and components that will be changed.

A conventional diesel fuel tank is located under the diesel engine at the bottom of the vehicle. The side view of the tank is trapezoidal, and its capacity is 8600 L of diesel, as shown in Figure 8. Firstly, the location of the fuel tank can be considered. Hydrogen leaks upwards in the case of fire, so it may be good to put the tank on top of the vehicle.

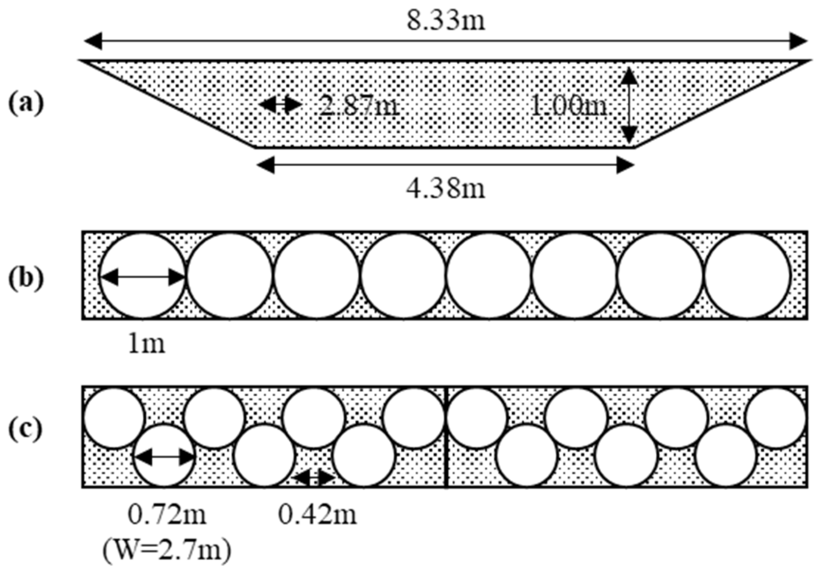

Figure 8. Fuel tank design: (**a**) size of a conventional diesel fuel tank at the bottom of the vehicle, (**b**) arrangement of 1-m-diameter tanks, and (**c**) arrangement of 0.72-m-diameter tanks.

Secondly, the design of the LH_2 tank can be considered. A vessel with a low surface-to-volume ratio shows a good insulation effect. However, the cylinder type is preferred to the sphere type because of the efficiency in space utilization. The cylindrical tank with a diameter of 0.72 m and a length of 2.7 m has a capacity of 500 L or 35 kg. If the tank space is a rectangular parallelepiped, 14 tanks (490 kg) can be stored. To enlarge the volumetric and energetic efficiency, the diameter of the cylinder tank can be 1 m or more. A larger tank can also offer better insulation (for example, 0.1 and 100 m^3 tanks show boil-off ratios of 2 and 0.06%, respectively [50]). The tank can be made in a spherical shape and placed inside the vehicle to maximize the thermal insulation effect. David et al. briefly reviewed the surface–volume ratio, boil-off ratio, and underlying assumptions of the LH_2 tank [51].

4.3. Structure and Efficiency of the Fuel Tank

The LH_2 tank design for aircraft and heavy-duty trucks (HDV) has been studied. Gomez et al. suggest structural sizing and stress analysis for EASA CS-25 aircraft [52]. Abu Kasim et al. suggest a performance and failure analysis for Cessna 208 aircraft [53]. Choi et al. reviewed the ISO 13985 tank for HDV [54]. The authors suggested a design procedure involving material selection and a structural and thermal analysis.

Thermodynamic analysis and CFD modeling of the LH_2 tank venting under microgravity have been studied. Shuang et al. suggested pressure control by using the microgravity of the tank, which showed that it can enhance the efficiency [55]. Jiang et al. did a CFD simulation of the tank's heat transfer and phase change under microgravity conditions. [56] Zheng et al. also did a CFD simulation of the tank under microgravity, but the authors added the dynamic results of the venting system [57]. Zuo et al. suggested a thermodynamic model of the venting process of an on-orbit structure liquid hydrogen tank [58].

5. Future Research Needs

In future studies, the approaches, as follows, are predicted to be available:

(1) The optimal suspension design between vessels and baffles in the inner vessel can be studied to minimize the BOG. Various CFD can be studied depending on the structure and vibration direction.

(2) The optimal location and method of filling and drain can be studied. Depending on the circumstances, the BOG in the charging process can be larger than the BOG in storage.

(3) Materials and arrangement of the vessel wall and insulation system can be studied. Former studies only focused on the insulation effect, but the optimal arrangement can exist depending on the operation, including filling and draining. A 4E analysis (Energy, Economic, Enthalpy, and Entropy) can be used.
(4) Dynamic control of the pressure, mass flow, and vaporizer (heat exchanger) system before the fuel cell can be studied.
(5) Utilizing the heat of the fuel cell or battery for heating the hydrogen in the vaporizer can also be studied.
(6) The arrangement of new components can be researched. For example, fuel cells and battery modules require a large cooling capacity. Liquid- or phase-change cooling can be applied.
(7) Various LH_2 vessel shapes, locations, and arrangements can be studied. The charger design is needed to research because of the large loss and BOG generation in the filling process.

6. Conclusions

Heavy-duty mobilities, including trains, are expected to change their fuel from fossil fuel to hydrogen, renewable energy for carbon-neutralization and solving global warming. The use of liquid hydrogen is one way to solve the low energy density of gaseous hydrogen. However, liquid hydrogen storage requires a high level of thermal insulation to minimize the boil-off gas.

This paper shows the recent hydrogen train research trend and reviews the thermodynamic modeling of the hydrogen tanks by dividing them into static, dynamic, and systematic levels. In static studies, insulation schemes, including IMs, MLIs, vessels, and vacuums, were researched. Thermal resistance diagrams involving hydrogen can be directly applied to dynamic studies. Regarding dynamic studies, the phase change of hydrogen was calculated. The shape, structure, and direction of the vibration of the tank were studied to check the boil-off ratio. Finally, systematic studies reviewed the surface–volume ratio and arrangement. The change of gravity and venting according to the arrangement also improved the system efficiency.

Author Contributions: Methodology, data curation, validation, and writing of the original draft, D.K.; conceptualization and investigation, S.Y.; and review and editing, B.-k.K. All authors have read and agreed to the published version of the manuscript.

Funding: This research was funded by a grant from the R&D program (PK2203F1) of the Korea Railroad Research Institute (KRRI).

Institutional Review Board Statement: Not applicable.

Informed Consent Statement: Not applicable.

Data Availability Statement: Not applicable.

Conflicts of Interest: The authors declare no conflict of interest.

References

1. Wijayanta, A.T.; Oda, T.; Purnomo, C.W.; Kashiwagi, T.; Aziz, M. Liquid hydrogen, methylcyclohexane, and ammonia as potential hydrogen storage: Comparison review. *Int. J. Hydrogen Energy* **2019**, *44*, 15026–15044. [CrossRef]
2. Wijayanta, A.T.; Nakaso, K.; Aoki, T.; Kitazako, Y.; Fukai, J. Effect of pressure, composition and temperature characteristics on thermal response and overall reaction rates in a metal hydride tank. *Int. J. Hydrogen Energy* **2011**, *36*, 3529–3536. [CrossRef]
3. Aziz, M. Liquid Hydrogen: A Review on Liquefaction, Storage, Transportation, and Safety. *Energies* **2021**, *14*, 5917. [CrossRef]
4. Hastings, L.J.; Hedayat, A.; Brown, T.M. *Analytical Modeling and Test Correlation of Variable Density Multilayer Insulation for Cryogenic Storage*; NASA: Washington, DC, USA, 2004.
5. Hastings, L.J.; Martin, J.J. Experimental testing of a foam/multilayer insulation (FMLI) thermal control system (TCS) for use on a cryogenic upper stage. *AIP Conf. Proc.* **1998**, *420*, 331–341.
6. Hedayat, A.; Hastings, L.J.; Brown, T. Analytical modeling of variable density multilayer insulation for cryogenic storage. *AIP Conf. Proc.* **2002**, *613*, 1557–1564.

7. Pehr, K.; Sauermann, P.; Traeger, O.; Bracha, M. Liquid hydrogen for motor vehicles-the world's first public LH2 filling station. *Int. J. Hydrogen Energy* **2001**, *26*, 777–782. [CrossRef]
8. Qiu, Y.; Yang, H.; Tong, L.; Wang, L. Research progress of cryogenic materials for storage and transportation of liquid hydrogen. *Metals* **2021**, *11*, 1101. [CrossRef]
9. Bergman, T.L.; Lavine, A.S.; Incropera, F.P.; DeWitt, D.P. *Fundamentals of Heat and Mass Transfer*; John Wiley & Sons: Hoboken, NJ, USA, 2011.
10. Polinski, J. *Materials in Cryogenics*; European Course in Cryogenics; CERN: Geneva, Switzerland, 2010.
11. Fesmire, J.E. Layered composite thermal insulation system for nonvacuum cryogenic applications. *Cryogenics* **2016**, *74*, 154–165. [CrossRef]
12. Johnson, W.; Fesmire, J. Thermal performance of low layer density multilayer insulation using liquid nitrogen. *AIP Conf. Proc.* **2012**, *1434*, 39–46.
13. Tseng, C.; Yamaguchi, M.; Ohmori, T. Thermal conductivity of polyurethane foams from room temperature to 20 K. *Cryogenics* **1997**, *37*, 305–312. [CrossRef]
14. Mekonnen, B.T.; Ding, W.; Liu, H.; Guo, S.; Pang, X.; Ding, Z.; Seid, M.H. Preparation of aerogel and its application progress in coatings: A mini overview. *J. Leather Sci. Eng.* **2021**, *3*, 25. [CrossRef]
15. Liu, Z.; Li, Y.; Zhou, G. Insulation performance of foam during the terrestrial and ascent period. *Appl. Therm. Eng.* **2018**, *145*, 364–374. [CrossRef]
16. Wang, P.; Liao, B.; An, Z.; Yan, K.; Zhang, J. Measurement and calculation of cryogenic thermal conductivity of HGMs. *Int. J. Heat Mass Transf.* **2019**, *129*, 591–598. [CrossRef]
17. Wang, P.; Ji, L.; Yuan, J.; An, Z.; Yan, K.; Zhang, J. Modeling and optimization of composite thermal insulation system with HGMs and VDMLI for liquid hydrogen on orbit storage. *Int. J. Hydrogen Energy* **2020**, *45*, 7088–7097. [CrossRef]
18. Andersson, J.; Grönkvist, S. Large-scale storage of hydrogen. *Int. J. Hydrogen Energy* **2019**, *44*, 11901–11919. [CrossRef]
19. Wang, P.; Ji, L.; Yuan, J.; An, Z.; Yan, K.; Zhang, J. The influence of inner material with different average thermal conductivity on the performance of whole insulation system for liquid hydrogen on orbit storage. *Int. J. Hydrogen Energy* **2021**, *46*, 10913–10923. [CrossRef]
20. Kim, T.Y.; Lee, J.H. Electromagnetic Shielding Effectiveness of CFRP Panels, MLI, and RF Screens for Spacecraft Applications. *J. Korean Inst. Electromagn. Eng. Sci.* **2020**, *31*, 947–955. [CrossRef]
21. Liu, Z.; Li, Y.; Xie, F.; Zhou, K. Thermal performance of foam/MLI for cryogenic liquid hydrogen tank during the ascent and on orbit period. *Appl. Therm. Eng.* **2016**, *98*, 430–439. [CrossRef]
22. Hedayat, A.; Brown, T.M.; Hastings, L.J.; Martin, J. Variable density multilayer insulation for cryogenic storage. In Proceedings of the 36th AIAA/ASME/SAE/ASEE Joint Propulsion Conference and Exhibit, Las Vegas, NV, USA, 24–28 July 2000.
23. Johnson, W.L. Thermal Performance of Cryogenic Multilayer Insulation at Various Layer Spacings. Master's Thesis, University of Central Florida, Orlando, FL, USA, 2010.
24. Johnson, W.L. Optimization of layer densities for multilayered insulation systems. *AIP Conf. Proc.* **2010**, *1218*, 804–811.
25. Wang, B.; Huang, Y.H.; Li, P.; Sun, P.J.; Chen, Z.C.; Wu, J.Y. Optimization of variable density multilayer insulation for cryogenic application and experimental validation. *Cryogenics* **2016**, *80*, 154–163. [CrossRef]
26. Zheng, J.; Chen, L.; Cui, C.; Guo, J.; Zhu, W.; Zhou, Y.; Wang, J. Experimental study on composite insulation system of spray on foam insulation and variable density multilayer insulation. *Appl. Therm. Eng.* **2018**, *130*, 161–168. [CrossRef]
27. Huang, Y.; Wang, B.; Zhou, S.; Wu, J.; Lei, G.; Li, P.; Sun, P. Modeling and experimental study on combination of foam and variable density multilayer insulation for cryogen storage. *Energy* **2017**, *123*, 487–498. [CrossRef]
28. Fesmire, J.E. Standardization in cryogenic insulation systems testing and performance data. *Phys. Procedia* **2015**, *67*, 1089–1097. [CrossRef]
29. Kuma, S.P.; Prasad, B.V.S.S.S.; Venkatarathnam, G.; Ramamurthi, K.; Murthy, S.S. Influence of surface evaporation on stratification in liquid hydrogen tanks of different aspect ratios. *Int. J. Hydrogen Energy* **2007**, *3*, 21954–21960.
30. Horie, Y.; Shirai, Y.; Shiotsu, M.; Matsuzawa, T.; Yoneda, K.; Shigeta, H.; Tatsumoto, H.; Hata, K.; Naruo, Y.; Kobayashi, H.; et al. Film boiling heat transfer properties of liquid hydrogen in natural convection. *Phys. Procedia* **2015**, *67*, 643–648. [CrossRef]
31. Baldwin, M.; Ghavami, A.; Ghiaasiaan, S.M.; Majumdar, A. Pool boiling in liquid hydrogen, liquid methane and liquid oxygen: A review of available data and predictive tools. *Cryogenics* **2021**, *115*, 103240. [CrossRef]
32. Ganesan, V.; Patel, R.; Hartwig, J.; Mudawar, I. Universal Critical Heat Flux (CHF) Correlations for Cryogenic Flow Boiling in Uniformly Heated Tubes. *Int. J. Heat Mass Transf.* **2021**, *166*, 120678. [CrossRef]
33. Kuang, Y.; Han, F.; Sun, L.; Zhuan, R.; Wang, W. Saturated hydrogen nucleate flow boiling heat transfer coefficients study based on artificial neural network. *Int. J. Heat Mass Transf.* **2021**, *175*, 121406. [CrossRef]
34. Wang, J.; Li, Y.; Wang, L. Numerical Study on Pool Film Boiling of Liquid Hydrogen over Horizontal Cylinders. *Energies* **2022**, *15*, 1044. [CrossRef]
35. Kang, B.H.; Kim, M.S. Prediction of evaporation loss through integrated modeling of liquid hydrogen storage tank. In *Proceedings of the Thermal Engineering Division Spring Conference, Jeju, Korea, 20–22 April 2022*; 22TE-Th06C12; Korean Society of Mechanical Engineers: Seoul, Korea, 2022.
36. Kang, D.H.; Na, S.I.; Yoo, J.W.; Lee, J.H.; Kim, M.S. Experimental study on the performance of a steam generation heat pump with the internal heat exchanging effect. *Int. J. Refrig.* **2019**, *108*, 154–162. [CrossRef]

37. Zheng, J.; Chen, L.; Wang, P.; Zhang, J.; Wang, J.; Zhou, Y. A novel cryogenic insulation system of hollow glass microspheres and self-evaporation vapor-cooled shield for liquid hydrogen storage. *Front. Energy* **2020**, *14*, 570–577. [CrossRef]
38. Lemmon, E.W.; Bell, I.H.; Huber, M.L.; McLinden, M.O. *NIST Standard Reference Database 23: Reference Fluid Thermodynamic and Transport Properties-REFPROP*; Version 10.0; National Institute of Standards and Technology, Standard Reference Data Program: Gaithersburg, MD, USA, 2018.
39. Jiang, W.B.; Zuo, Z.Q.; Huang, Y.H.; Wang, B.; Sun, P.J.; Li, P. Coupling optimization of composite insulation and vapor-cooled shield for on-orbit cryogenic storage tank. *Cryogenics* **2018**, *96*, 90–98. [CrossRef]
40. Jiang, W.; Sun, P.; Li, P.; Zuo, Z.; Huang, Y. Transient thermal behavior of multi-layer insulation coupled with vapor cooled shield used for liquid hydrogen storage tank. *Energy* **2021**, *231*, 120859. [CrossRef]
41. Zheng, J.; Chen, L.; Wang, J.; Zhou, Y.; Wang, J. Thermodynamic modelling and optimization of self-evaporation vapor cooled shield for liquid hydrogen storage tank. *Energy Convers. Manag.* **2019**, *184*, 74–82. [CrossRef]
42. Jeon, G.M.; Park, J.C.; Choi, S. Multiphase-thermal simulation on BOG/BOR estimation due to phase change in cryogenic liquid storage tanks. *Appl. Therm. Eng.* **2021**, *184*, 116264. [CrossRef]
43. Liu, Z.; Feng, Y.; Lei, G.; Li, Y. Fluid thermal stratification in a non-isothermal liquid hydrogen tank under sloshing excitation. *Int. J. Hydrogen Energy* **2018**, *43*, 22622–22635. [CrossRef]
44. Liu, Z.; Li, C. Influence of slosh baffles on thermodynamic performance in liquid hydrogen tank. *J. Hazard. Mater.* **2018**, *346*, 253–262. [CrossRef]
45. Liu, Z.; Feng, Y.; Lei, G.; Li, Y. Fluid sloshing dynamic performance in a liquid hydrogen tank. *Int. J. Hydrogen Energy* **2019**, *44*, 13885–13894. [CrossRef]
46. Wei, G.; Zhang, J. Numerical Study of the Filling Process of a Liquid Hydrogen Storage Tank under Different Sloshing Conditions. *Processes* **2020**, *8*, 1020. [CrossRef]
47. Ghafri, S.Z.S.A.; Swanger, A.; Jusko, V.; Siahvashi, A.; Perez, F.; Johns, M.L.; May, E.F. Modelling of Liquid Hydrogen Boil-Off. *Energies* **2022**, *15*, 1149. [CrossRef]
48. Petitpas, G. *Boil-off Losses along LH2 Pathway*; LLNL-TR-750685; Lawrence Livermore National Laboratory: Livermore, CA, USA, 2018.
49. Smith, J.R.; Gkantonas, S.; Mastorakos, E. Modelling of Boil-Off and Sloshing Relevant to Future Liquid Hydrogen Carriers. *Energies* **2022**, *15*, 2046. [CrossRef]
50. Godula-Jopek, A.; Jehle, W.; Wellnitz, Z. *Hydrogen Storage Technologies: New Materials, Transport and Infrastructure*; Wiley-VCH: Weinheim, Germany, 2012.
51. David, B.; Stefania, G.; Simon, R.; Mari, V.; Yuki, I.; Petter, N. Liquid hydrogen as prospective energy carrier: A brief review and discussion of underlying assumptions applied in value chain analysis. *Renew. Sustain. Energy Rev.* **2022**, *154*, 111772.
52. Gomez, A.; Smith, H. Liquid hydrogen fuel tanks for commercial aviation: Structural sizing and stress analysis. *Aerosp. Sci. Technol.* **2019**, *95*, 105438. [CrossRef]
53. Abu Kasim, A.F.B.; Chan, M.S.C.; Marek, E.J. Performance and failure analysis of a retrofitted Cessna aircraft with a Fuel Cell Power System fuelled with liquid hydrogen. *J. Power Source* **2022**, *421*, 230987. [CrossRef]
54. Choi, Y.; Kim, J.; Park, S.; Park, H.; Chang, D. Design and analysis of liquid hydrogen fuel tank for heavy duty truck. *Int. J. Hydrogen Energy* **2022**, *47*, 14687–14702. [CrossRef]
55. Shuang, J.J.; Liu, Y.W. Efficiency analysis of depressurization process and pressure control strategies for liquid hydrogen storage system in microgravity. *Int. J. Hydrogen Energy* **2019**, *44*, 15949–15961. [CrossRef]
56. Jiang, Y.; Yu, Y.; Wang, Z.; Zhang, S.; Cao, J. CFD simulation of heat transfer and phase change characteristics of the cryogenic liquid hydrogen tank under microgravity conditions. *Int. J. Hydrogen Energy* **2022**, in press. [CrossRef]
57. Zheng, Y.; Yang, P.; Liu, Y.; Yang, Q.; Yan, C.; Wang, X. Parametric optimization and analysis of thermodynamic venting system in liquid hydrogen tank under microgravity. *Int. J. Hydrogen Energy* **2021**, *46*, 40041–40053. [CrossRef]
58. Zuo, Z.; Jiang, W.; Qin, X.; Huang, Y. Numerical investigation on full thermodynamic venting process of liquid hydrogen in an on-orbit storage tank. *Int. J. Hydrogen Energy* **2020**, *45*, 27792–27805. [CrossRef]